Motion of Long Levitating Drops in Tubes in an Anti-Bretherton Configuration

Peter Favreau,[1] Alexis Duchesne,[1] Farzam Zoueshtiagh,[1] and Michaël Baudoin[1,2,*]
[1]Université Lille, CNRS, Centrale Lille, ISEN, Université Valenciennes, IEMN UMR 8520, F-59000 Lille, France
[2]Institut Universitaire de France, 1 rue Descartes, 75231 Paris Cedex 05, France

(Received 26 February 2020; accepted 7 October 2020; published 2 November 2020)

In his seminal paper, Bretherton studied the motion of long bubbles in capillary tubes. Here, we unveil the negative configuration wherein a long liquid drop is stably transported in a capillary tube and surrounded by a flow-induced air cushion. These drops are formed when a liquid plug is pushed above a critical velocity sufficient to induce an inversion of the front meniscus with a radius of curvature smaller than the tube radius. The drop shape and lubricating air film thickness is reminiscent of Bretherton's calculation and can be inferred from an adapted analytical theory.

DOI: 10.1103/PhysRevLett.125.194501

In his 1961 seminal paper [1], Bretherton studied experimentally and theoretically the motion of long bubbles in capillary tubes in the limit of creeping flows, i.e., at low Reynolds and capillary numbers. This configuration was first explored in millimetric tubes at very low flow rates or with highly viscous fluids. Then, the emergence of microfluidics [2,3] led to some renewed interest in Bretherton's theory, owing to its relevance to various two-phase flow configurations at small scales, including bubbles [1,4,5], plugs [6–11], and foam [12–14] dynamics in capillary tubes. Moreover, his theory was extended later on to a larger range of flow parameters, e.g., larger capillary and Reynolds numbers [15–17], more complex tube geometry [18–20], or non-Newtonian embedding liquids [21,22]. In this Letter, we investigate experimentally, theoretically, and numerically the negative of Bretherton's configuration, i.e., a long liquid drop moving in an air-filled cylindrical tube, whose contact with the walls is prevented by a self-induced air cushion. First, we show experimentally and numerically that these levitating drops can be formed by pushing a liquid plug inside a microfluidic channel at a capillary number large enough to induce an inversion of the meniscus with a radius of curvature smaller than the radius of the tube. Second, we develop an analytical model that is able to recover the shape and thickness of the air lubricating film at walls in the limit of low (air) capillary numbers. Finally, we explore a larger set of parameters and draw a phase diagram delimiting the regimes in which long levitating droplets are formed. While systems designed to synthesize bubbles or drops in liquids are ubiquitous in microfluidics [23–25], the formation of long levitating drops in air has only been reported in hydrophobic channels [26], wherein contact with the walls is prevented by the specific surface treatment. This work provides a simple way to generate long drops of controlled length stably propagating in regular tubes, which may serve in digital microfluidics to transport liquids without any wall contamination.

Methods and results.—Experimentally, a long levitating drop is synthesized inside a glass cylindrical capillary tube of radius $R = 0.5$ mm (i) by injecting with a needle a controlled amount of silicone oil in the tube leading to the formation of a liquid plug, as depicted in Fig. 1(a), and (ii) by pushing this liquid plug with a large constant air flow rate Q in the range 1–50 mL/ min. The tubes were carefully cleaned prior to experiments with acetone, isopropyl alcohol, and dichloromethane to obtain perfectly wetting walls. The plug and then droplet evolution are recorded at 10 000 or 15 000 frames per second with a high speed camera (Photron SA3) mounted on a Leica Z16 macroscope [Fig. 1(a) and video M1 in the Supplemental Material [27]]. At rest (Image 0), the plug front and rear menisci are two opposite half-spheres tangent to the walls, which fulfills both the Young–Laplace law (leading to spherical liquid and air interfaces) and the perfectly wetting condition of silicone oil on the walls (leading to a 0° contact angle). Then, a flow rate sufficient to induce an inversion of the curvature of the front interface with a radius of curvature smaller than the tube radius is imposed (Image 1). This leads to the formation of a thin air film surrounding the front part of the liquid plug, as evidenced by the grayer color of the liquid (indicating that the liquid is no longer contacting the walls). The thin film of air extends progressively downward around the plug (Image 2) until it contacts the rear interface of the plug (Image 3), leading to the detachment of the drop, which then propagates stably in the tube (Image 4). The shape of the drop evokes the shape of Bretherton's bubble [1] with a phase inversion. Note that, to improve the repeatability of the experiments and ease the comparison with the simulations (i.e., avoid contact line problems), the walls were prewetted prior to the experiments by injecting a liquid plug inside the channel and pushing it with a low constant flow rate $Q = 4.5$ μL/ min (corresponding to a low capillary number $Ca_l \approx 4.6 \times 10^{-4}$), leading to the deposition on the walls of a thin liquid film of

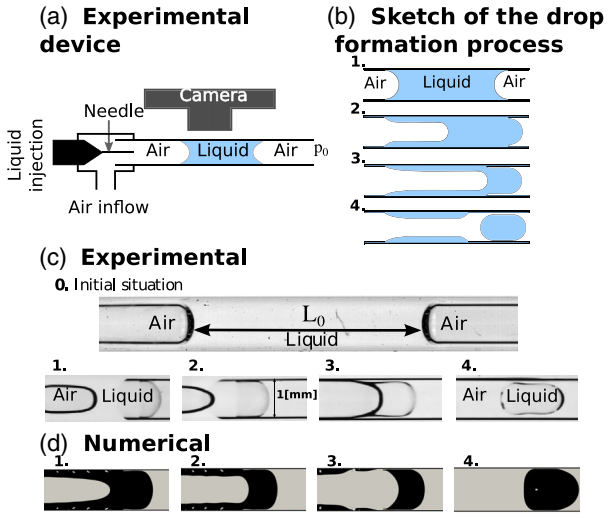

FIG. 1. Transition from a liquid plug to a long levitating drop. (a) Sketch of the experimental device. (b) Sketch of the drop formation process. (c) Snapshot of an experiment: a 10^{-4} m^2 s^{-1} silicone oil liquid plug of length 19 mm is pushed inside a capillary tube of radius $R = 0.5$ mm by a constant flow of air ($Q = 11$ mL/ min) with a syringe pump, leading to a velocity of the rear interface U of 0.6 ms^{-1} (corresponding to a capillary number $Ca_l = (\mu_l U/\sigma) = 2.8$, with μ_l the liquid dynamic viscosity and σ the surface tension). Image 0 shows the initial plug shape before actuation. Image 1 ($t = 0$ ms) shows the deformed rear interface and the inverted front interface when the plug is pushed by a flow of air. Image 2 ($t = 0.6$ ms) shows the evolution of the liquid plug and the appearance of a thin film of air surrounding the liquid at the front of the plug. Image 3 shows ($t = 2.3$ ms) the drop detachment, and Image 4 shows the detached long liquid drop stably propagating in the tube. (d) Numerical simulation of the previous experiment with the same flow parameters: black is silicone oil, white is air.

controlled thickness [1,9] $h_p = 0.643R(3Ca_l)^{2/3} \approx 4$ μm, with R the radius of the capillary tube, $Ca_l = (\mu_l U/\sigma)$ the capillary number of the liquid comparing viscous effects to surface tension ones, μ_l the liquid dynamic viscosity, and U the speed of the rear interface of the plug. More details about the experimental procedure are given in Section II of the Supplemental Material [27]. Numerically, the same dynamics [Fig. 1(c)] is simulated in a 2D axisymmetric configuration with a volume of fluid method [28] implemented in the open-source code OpenFOAM, solving the following set of equations:

$$\nabla \cdot \boldsymbol{u} = 0,$$
$$\partial_t \rho \boldsymbol{u} + \nabla \cdot (\rho \boldsymbol{u} \otimes \boldsymbol{u}) = -\nabla(p) + \mu \Delta(\boldsymbol{u}) + \sigma \kappa \boldsymbol{n} \delta_S,$$
$$\partial_t \alpha + \nabla \cdot (\alpha \boldsymbol{u}) = 0,$$
$$\rho = \alpha \rho_l + (1-\alpha)\rho_g; \qquad \mu = \alpha \mu_l + (1-\alpha)\mu_g,$$

where σ is the surface tension, μ_i and ρ_i the viscosity and density of the phase i, ($i = l$ for the liquid and g for the gas), $\boldsymbol{u}$ the fluid velocity, and p the dynamic pressure. α is a phase marker equal to 0 in the gas and 1 in the liquid. The interface between the two fluids thus corresponds to $\alpha \in [0, 1]$. The initial and boundary conditions are detailed in Section IV of the Supplemental Material [27]. The term taking into account the effects of surface tension is $\sigma \kappa \boldsymbol{n} \delta_S$, with δ the Kronecker symbol, equal to 1 on the interface. This modeling was introduced by Brackbill *et al.* [29] and called the continuum surface force model. Since the volume of fluid method is known to generate parasitic currents [30–32], i.e., spurious hydrodynamic vortices close to the interface, a restrictive time step was imposed to guarantee the stability of this parasitic flow [33] $\Delta t \leq \max\left[0.1\sqrt{\rho \Delta x^3/\sigma}; 10(\mu \Delta x/\sigma)\right]$, with Δx the characteristic length of a mesh cell. We also implemented an adaptive mesh in the code. Indeed, the correct calculation of the flow close to the walls and interfaces requires a refined mesh for the sake of precision. Without adaptive mesh, the calculation cost would be prohibitive.

Transition from liquid plug to long levitating drop.—The dynamics of liquid plugs in perfectly wetting channels has been widely studied experimentally [8,9,34], numerically [35–37], and theoretically [6–8,10,11,38]. From a theoretical perspective, a liquid plug can be seen as a bridge of liquid trapped between two semi-infinite air bubbles. Hence, the laws of deformation of the front (respectively rear) interface of a liquid plug can be inferred from corresponding laws derived for the deformation of the rear (respectively front) interface of long bubbles [1,4,39,40]. Nevertheless, most studies have been conducted in the analytically tractable low or intermediate [15,16] capillary number limit, wherein the curvature sign of the meniscus is not changed.

Hoffman [41] studied experimentally the evolution of the front meniscus of an advancing liquid finger on a large range of liquid capillary numbers (ranging from $\approx 4 \times 10^{-5}$ to ≈ 35). He reported an evolution of the apparent contact angle from $\approx 5°$ to $\approx 180°$, corresponding to an inversion of the front meniscus curvature from $C \approx -2/R$ to $C \approx 2/R$ (with R the radius of the tube). This behavior was rationalized later on by Boender *et al.* [42] with approximate analytical models. Here we show both experimentally [Fig. 1(b)] and numerically [Fig. 2(a),(c)] that when the capillary number exceeds a critical capillary number Ca_l^c at which the radius of curvature becomes equal to the tube radius R (or more precisely $R - h_p$ in this Letter owing to the existence of a prewetting film), the radius of curvature continues to decrease (while more slowly) through the appearance of a thin air film that fills the gap between the front meniscus and the walls [Fig. 2(c)]. The appearance of this film of air is the key ingredient in the formation of long levitating drops from the fast dynamics of liquid plugs. Indeed, this film of air extends progressively backward [Fig. 1(b)] until it reaches the back of the drop, hence provoking its detachment. Interestingly, this deposition of a

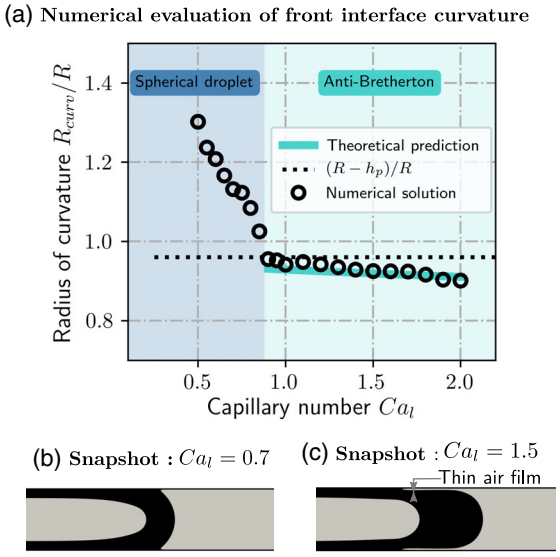

FIG. 2. Thin air film formation above a critical capillary number. (a) Numerical evaluation of the front interface curvature R_{curv} of the front interface of a liquid plug divided by the tube radius R as a function of the capillary number Ca_l (at constant Ohnesorge number $Oh = 0.4$). When the radius of the curvature exceeds the tube radius [snapshot (b)], spherical droplets are formed when the plug ruptures. When the plug becomes smaller than the tube radius (above a critical capillary number), a thin film of air appears between the plug and the walls [snapshot (c)] leading to the formation of an anti-Bretherton drop. (b) Snapshot of numerical simulation: $Ca_l = 0.7$, $Oh = 0.4$. (c) Snapshot of numerical simulation: $Ca_l = 1.5$, $Oh = 0.4$.

thin air film behind the drop front interface is reminiscent of the deposition of a thin film of liquid behind the front interface of a bubble predicted by Bretherthon's theory but with a phase inversion.

Thin air film thickness prediction: anti-Bretherton.— Since these two configurations share some similarities, we derived a model to evaluate the thickness of the air film as a function of the capillary number by following a similar procedure as the one proposed by Bretherton. First, it is important to stress that two capillary numbers are involved in this problem: one based on the gaseous phase $Ca_g = \mu_g U/\sigma$ and one based on the liquid $Ca_l = \mu_l U/\sigma$. Of course these are proportional to each other, $Ca_g = \mu_g/\mu_l Ca_l$, with a constant depending on the gas and liquid viscosity ratio. The condition for the formation of an anti-Bretherton drop from a liquid plug imposes that $Ca_l > Ca_l^c \sim \mathcal{O}(1)$ since viscous stresses must overcome surface tension to induce an inversion of the front interface up to a point wherein the radius of curvature becomes smaller than the radius of the tube. On the other hand, the thickness of the film of air appearing behind the drop front interface relies on the capillary number in the air Ca_g. This capillary number remains small (Ca_g in the range 10^{-4} to 10^{-2}) in all the simulations and experiments provided in this Letter, as well as the Reynolds number associated with the flow in the air film (Re_g in the range 10^{-3} to 2). Hence, the classic lubrication approximation can be used to describe the flow in the thin air film:

$$\begin{cases} \partial_x p_g = \mu_g \partial^2_{yy} u_x \\ \partial_y p_g = 0 \end{cases} \Rightarrow \frac{dp_g}{dx} = \mu_g \frac{d^2 u_x}{dy^2}, \tag{1}$$

with u_x and p_g the longitudinal velocity and pressure in the air film. We adopt here a quasi-2D approximation of the axisymmetric problem. This approximation was introduced and thoroughly justified by Bretherton in his paper [1] and holds as long as the capillary number is small, leading to the deposition of a thin film compared to the tube radius. For intermediate capillary numbers, the modified Laplace pressure must be used, leading to the Ausillous and Quére equation [15,16]. Owing to the large difference of viscosity between the fluid and the air, the thin prewetting film of liquid on the walls can be considered at rest, and the velocity inside the detaching drop can be considered as constant. This approximation is discussed in detail in Section III of the Supplemental Material [27] and confirmed by the numerical simulations. Hence, in the drop frame of reference, the boundary conditions at the walls (or more precisely the prewetting film surface) becomes $u_x(y = 0) = -U$ with U the drop speed, while at the interface between the film and the drop, i.e., at $y = h(x)$, we have $u_x[h(x)] = 0$ where $h(x)$ denotes the thickness of the air film. See Section III of the Supplemental Material [27] for a detailed discussion of these boundary conditions. The normal stress balance at the drop interface gives $p = -\sigma\{(1/R) + [d^2h(x)/dx^2]\}$, with $p = p_g - p_l$, where p_g and p_l are the pressures in the gas and liquid phase, respectively. Finally, the mass conservation in the air film gives $\int_0^{h(x)} u_x dy = -UH$, with H the constant thickness of the film far from the drop front meniscus. The only difference from the equations derived by Bretherton is the boundary condition at $y = h(x)$, which for a drop (present case) is an adherence condition $u_x[h(x)] = 0$, while for a bubble is a zero stress condition. The combination of these equations with the change of variable $x = H(12Ca_g)^{-1/3}\xi$ and $h(x) = H\psi$ leads to the celebrated Landau–Levich equation [1,43]:

$$\frac{d^3\psi}{d\xi^3} = \frac{\psi - 1}{\psi^3}. \tag{2}$$

This equation coincides with the one obtained by Bretherton except for the coefficient in the change of variable $x = H(12Ca_g)^{-1/3}\xi$, which is 12 instead of 3 for a bubble. Hence, we can infer the thickness of the film of air from the solution obtained by Bretherton by a simple change of coefficient:

$$\frac{h_a}{R} = 0.643(12Ca_g)^{2/3}. \tag{3}$$

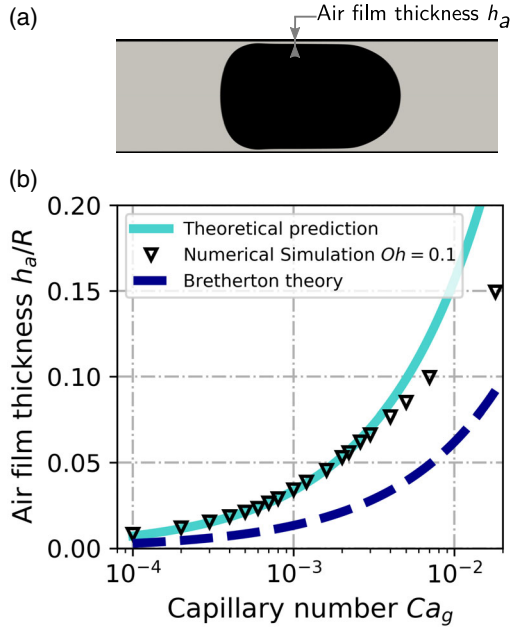

FIG. 3. Lubricating air film thickness. (a) Simulation showing a long levitating drop moving in a capillary tube and separated from the walls by a thin air film of thickness h_a (b) Evaluation of the thickness of the air film h_a as a function of the air capillary number Ca_g. Triangles: numerical simulation. Cyan continuous line: adapted Bretherton theory for levitating drops. Blue dashed line: Bretherton's theory for bubbles.

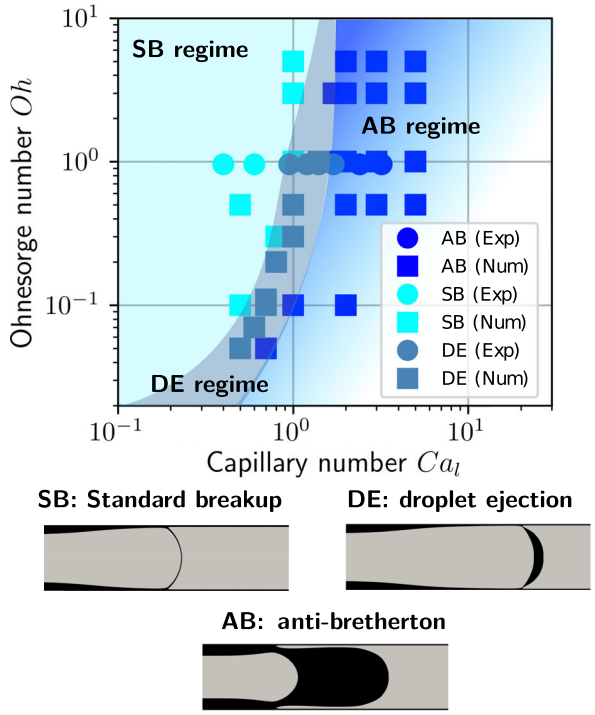

FIG. 4. Phase diagram summarizing the regimes observed experimentally and numerically for different capillary and Ohnesorge numbers. Standard breakup (SB): the plug breaks from the center with no plug formation. Droplet ejection (DE): a spherical drop is ejected at the center of the channel. Anti-Bretherton (AB): a long levitating drop separated from the walls by an air cushion is formed (see video M2 in the Supplemental Material [27]).

The validity of this analytical expression was verified through comparison to numerical simulations of the dynamics of long drops in capillary tubes resulting from the rupture of a liquid plug at high liquid capillary numbers (Fig. 3). The thickness of the film was measured in the flat part of the drop away from the menisci. The results of the simulation are presented in Fig. 3 (triangles) and compared to both the present analytical expression (cyan continuous line) and the result obtained by Bretherton for bubbles (purple dashed line). The analytical expression obtained is in excellent agreement with the simulations in the limit of low capillary numbers $Ca_g < 3 \times 10^{-3}$ and differs, as expected, from the simulations for larger capillary numbers [15]. Note that the effect of gravity could not be considered in the axisymmetric simulations. Nevertheless, owing to the large density of the liquid compared to air, gravity could lead to a thinner film below than above the drop. This effect was not noticed experimentally since the drop motion in the horizontal channel was visualized only from the top and not laterally. Note also that the adherence condition at the air and liquid interface leads to shear stresses all along the film (while the film is at rest in the bubble case away from the dynamic meniscus). Hence the associated pressure drop is expected to induce a continuous variations of the air film thickness for long drops.

Phase diagram.—We further investigated experimentally and numerically the regimes leading to the formation of long anti-Bretherton drops on a large set of parameters. Since the three effects at stake are viscous, inertial, and capillary effects, a phase diagram can be plotted as a function of two dimensionless numbers: the capillary number $Ca_l = \mu_l U/\sigma$ and the Ohnesorge number $\mathcal{O}_h = \mu_l/\sqrt{\rho_l \sigma R}$ (see Fig. 4). The Ohnesorge number compares viscous effects stabilizing an interface to the geometric average of destabilizing inertial and capillary effects. In the range of capillary numbers sufficient to have an inversion of the front interface curvature, three regimes can be observed (see Fig. 4 and video M2 in the Supplemental Material [27]): (i) a regime named "standard breakup" (SB) wherein the liquid plug becomes thinner and thinner until it breaks with no droplet production. This regime occurs when the radius of curvature of the front interface remains larger than the tube radius. (ii) An intermediate regime named "droplet ejection" (DE) wherein a small drop is ejected when the front interface radius of curvature is almost equal to the tube radius. And finally (iii), the "anti-Bretherton" large drop production regime leading to the production of a long droplet separated from the tube walls by a thin air film. This regime (as discussed before) occurs when the radius of curvature of the front interface becomes smaller than the tube radius. Note that the length of the

ejected droplet depends quasilinearly on the initial plug length (for sufficiently long plugs) but with a slope that depends on the capillary number (see Section V in the Supplemental Material [27]). This provides a means to control the droplet length.

Conclusion.—In this Letter, we study experimentally, theoretically, and numerically the dynamics of large drops levitating in a capillary tube, produced by the rupture of a liquid plug. We show that the production of these large drops occurs when a liquid plug is pushed above a critical speed, sufficient to lead to an inverted front meniscus with a radius of curvature smaller than the tube radius. This leads to the development of a thin air film between the plug and the walls, propagating downward the plug until its complete detachment. The resulting drops' shapes are reminiscent of the shape of the long bubble propagating in a liquid filled tube and can be inferred from Bretherton's model with inverted phases and adapted boundary conditions. This Bretherton-like transportation mode enables high speed stable contactless drop transport with reduced friction and no wall contamination. During the drop formation phase, however, some liquid is initially deposited on the walls. Hence to obtain an entirely contamination free process, either the drop production unit could be separated from the transport part by using cross junctions or the potential of other drop synthesis systems to produce long droplets, such as flow focusing (with high speed air flow), could be investigated.

This work was supported by ISITE-ULNE (ERC generator program) and Institut Universitaire de France.

*Corresponding author.
michael.baudoin@univ-lille.fr

[1] F. Bretherton, J. Fluid Mech. **10**, 166 (1961).
[2] H. Stone, A. Stroock, and A. Ajdari, Annu. Rev. Fluid Mech. **36**, 381 (2004).
[3] T. M. Squires and S. R. Quake, Rev. Mod. Phys. **77**, 977 (2005).
[4] C.-W. Park and G. Homsy, J. Fluid Mech. **139**, 291 (1984).
[5] M. Prakash and N. Gershenfeld, Science **315**, 832 (2007).
[6] D. Halpern, O. Jensen, and J. Grotberg, J. Appl. Phys. **85**, 333 (1998).
[7] P. Howell, S. Waters, and J. Grotberg, J. Fluid Mech. **406**, 309 (2000).
[8] M. Baudoin, Y. Song, P. Manneville, and C. N. Baroud, Proc. Natl. Acad. Sci. U.S.A. **110**, 859 (2013).
[9] J. Magniez, M. Baudoin, C. Liu, and F. Zoueshtiagh, Soft Matter **12**, 8710 (2016).
[10] F. Xu and O. E Jensens, Phys. Rev. Fluids **2**, 094004 (2017).
[11] S. S. Mamba, J. Magniez, F. Zoueshtiagh, and M. Baudoin, J. Fluid Mech. **838**, 165 (2018).
[12] I. Cantat, N. Kern, and R. Delannay, Europhys. Lett. **65**, 726 (2004).
[13] N. Denkov, V. Subramanian, D. Gurovich, and A. Lips, Colloids Surf. A **263**, 129 (2005).
[14] R. Höhler and S. Cohen-Addad, J. Phys. Condens. Matter **17**, R1041 (2005).
[15] P. Aussillous and D. Quéré, Phys. Fluids **12**, 2367 (2000).
[16] E. Klaseboer, R. Gupta, and R. Manica, Phys. Fluids **26**, 032107 (2014).
[17] A. Cherukumudi, E. Klaseboer, S. Khan, and R. Manica, Microfluid. Nanofluid. **19**, 1221 (2015).
[18] H. Wong, C. Radke, and S. Morris, J. Fluid Mech. **292**, 71 (1995).
[19] H. Wong, C. Radke, and S. Morris, J. Fluid Mech. **292**, 95 (1995).
[20] A. L. Hazel and M. Heil, J. Fluid Mech. **470**, 91 (2002).
[21] M. Jalaal and N. Balmforth, J. Non-Newtonian Fluid Mech. **238**, 100 (2016).
[22] B. Labories, F. Rouyer, D. Angelescu, and E. Lorenceau, J. Fluid Mech. **818**, 838 (2017).
[23] S. Anna, N. Bontoux, and H. Stone, App Phys. Lett. **82**, 364 (2003).
[24] P. Garstecki, M. Fuerstman, H. Stone, and G. Whitesides, Lab Chip **6**, 437 (2006).
[25] T. Nisiako, T. Torii, and Y. Takizawa, Adv. Mater. **18**, 1152 (2006).
[26] P. Tirandazi and C. H. Hidrovo, J. Micromech. Microeng. **27**, 075020 (2017).
[27] See Supplemental Material at http://link.aps.org/supplemental/10.1103/PhysRevLett.125.194501 for additional details on the experiments, theoretical model and numerical procedure.
[28] C. W. Hirt and B. D. Nichols, J. Comput. Phys. **39**, 201 (1981).
[29] J. Brackbill, D. B. Kothe, and C. Zemach, J. Comput. Phys. **100**, 335 (1992).
[30] T. Abadie, J. Aubin, and D. Legendre, J. Comput. Phys. **297**, 611 (2015).
[31] M. M. Francois, S. J. Cummins, E. D. Dendy, D. B. Kothe, J. M. Sicilian, and M. W. Williams, J. Comput. Phys. **213**, 141 (2006).
[32] D. J. Harvie, M. Davidson, and M. Rudman, Appl. Math. Model. **30**, 1056 (2006).
[33] S. S. Deshpande, L. Anumolu, and M. F. Trujillo, Comput. Sci. Discovery **5**, 014016 (2012).
[34] S. Signé Mamba, J. Magniez, F. Zoueshtiagh, and M. Baudoin, Int. J. Multiphase Flow **113**, 343 (2019).
[35] H. Fujioka and J. B. Grotberg, Phys. Fluids **17**, 082102 (2005).
[36] H. Fujioak, S. Takayama, and J. Grotberg, Phys. Fluids **20**, 062104 (2008).
[37] E. A. Hassan, E. Uzgoren, H. Fujioka, J. B. Grotberg, and W. Shyy, Int. J. Numer. Methods Fluids **67**, 1373 (2011).
[38] O. Jensen, J. Colloid Interface Sci. **221**, 38 (2000).
[39] J. Ratulowski and H.-C. Chang, Phys. Fluids A **1**, 1642 (1989).
[40] V. S. Ajaev and G. Homsy, Annu. Rev. Fluid Mech. **38**, 277 (2006).
[41] R. L. Hoffman, J. Colloid Interface Sci. **50**, 228 (1975).
[42] W. Boender, A. Chesters, and A. Van Der Zanden, Int. J. Multiphase Flow **17**, 661 (1991).
[43] B. Levich and L. Landau, Acta Physicochimica U.R.S.S. **XVII**, 42 (1942).